Supporting Information

Intrinsically Reversible Superglues via Shape Adaptation Inspired by Snail Epiphragm

Hyesung Cho[1,†], Gaoxiang Wu[1,†], Jason Christopher Jolly[1,†], Nicole Fortoul[2], Zhenping He[2], Yuchong Gao[1], Anand Jagota[2,*], and Shu Yang[1,*]

[1]Department of Materials Science and Engineering, University of Pennsylvania, 3231 Walnut Street, Philadelphia, PA 19104, United States.

[2]Departments of Chemical & Biomolecular Engineering and Bioengineering, Lehigh University, 111 Research Drive, Bethlehem, PA 18105, United States.

*Correspondence to: shuyang@seas.upenn.edu (S. Yang) and anj6@lehigh.edu (A. Jagota)

[†]These authors contributed equally to this work.

Sample selection for indentation

The moduli of the PHEMA hydrogel in both wet and dry states were characterized by atomic force microscopy (AFM). Samples with 2 vol% and 8 vol% of the crosslinker, EGDMA, showed similar values of moduli at hydrated (~ 180 kPa) and dry (~ 2.3 GPa) states as seen in **Fig. S1**. Note that the value in wet state is near-surface value due to an oxygen inhibition effect as a consequence of the samples being cured under an oxygen permeable polydimethylsiloxane (PDMS) mold. In the case of samples from 2 vol% crosslinkers, after solvent exchange to remove the uncrosslinked monomers for indentation measurement, dimples and voids are observed at the surface of the crosslinked gel due to low crosslinking density, leading to significant variability during indentation tests with an applied preload of ~ 100 mN. Since the hydrogels with 2 vol% and 8 vol% EDGMA showed similar near-surface moduli and our primary purpose is to understand the adhesion mechanism and tunability via a single asperity, that is modulus in the wet state vs. in the dry state,

here, we chose to focus on 8 vol% samples in indentation studies. The small near-surface modulus (~ 180 kPa) helped make conformal contact against a rough surface despite the relatively high bulk modulus (~ 35 MPa, see **Fig. S2** and discussion below). In the case of macroscale demonstration and measurement, we circumvented the issues in samples with 2 vol% EGDMA using a higher preload ~ 5 N, rendering the effect of dimples and voids negligible.

Measurement of the bulk elastic modulus of wet, PHEMA samples, 8 vol% EGDMA.

A non-pattered PHEMA film (thickness of 125 μm) under dry and wet conditions was indented as controls with a spherical glass indenter (R ~ 3.025 mm, **Fig. S2-S5**). From the normal load (P) versus deflection (δ, indentation depth) curve, the Young's modulus of the hydrogel was determined. Due to the internal spring within the load cell, the displacement of the motor was greater than the displacement of the indenter during indentation. The discrepancy between the motor displacement and the indenter displacement was accounted for using the spring constant of the load cell, 1773 N/m. δ can be written as a function of P, R, and plane strain Youngs modulus (E^*)(1),

$$\delta^3 = \frac{9P^2}{16RE^{*2}} \qquad (S1)$$

The Young's Modulus, E, of an incompressible material is related to E^* through

$$E^* = \frac{4E}{3} \qquad (S2)$$

Combining Eqs. S1 and S2, we obtain

$$E = \frac{9}{16\sqrt{R}}\frac{P}{\delta^{3/2}} \qquad (S3)$$

$\frac{P}{\delta^{3/2}}$ was calculated using the slope of P versus $\delta^{3/2}$ from the wet indentation experiment. A linear fit of the curve in **Fig. S2** was used to calculate $\frac{P}{\delta^{3/2}}$ as 10,8029 mN/mm$^{3/2}$. Inputting this value in Eq. S3 yields E for a wet PHEMA film, to be 34.9 MPa.

Accounting for finite layer thickness in theoretical treatment of pull-off force. As described in the main text (Eq. 1), pull-off force during indentation in the wet state was interpreted using the Johnson-Kendall-Roberts (JKR) model(2) for adhesive contact between a smooth spherical indenter and an elastic surface. Pull-off in the post-dried state was interpreted using the elastic solution for a flat punch (Eq.2). Both equations need to be corrected if the contact radius is significantly larger than the film thickness. The relationship between energy release rate (and so the work of adhesion, *W)*, and pull-off force, *F,* can be described as(3)

$$F = \sqrt{2W\frac{dA}{dC}} \tag{S4}$$

where A is the cracked area, and C is the system compliance. According to the JKR model, the corresponding relationship is(4)

$$F = F_H + \sqrt{2W\frac{dA}{dC}} \tag{S5}$$

where F_H is the "Hertz" load, or the force required to achieve the same contact area without adhesion. The primary quantity to examine when considering whether and what correction needs to be made is $\frac{dA}{dC}$. In this instance, *C(A)* is the compliance of a rigid punch adhered to the surface of the sample. Long *et al*(5). have provided an expression for compliance:

$$C = C_\infty \left[\frac{1}{1+f(\eta)}\right]$$

where $f(\eta) = \frac{1.095\,\eta + 1.3271\,\eta^2 + 0.1431\,\eta^3}{0.9717}$; $\eta = \frac{a}{h}$; $A = \pi a^2$ (S6)

Using these relations together with the measured values of contact area at pull-off and film thickness, we find that for wet indentation (**Fig. S4**), the value of d*C*/dA differs from that for a semi-infinite half space by less than 10%. Therefore, Eq. (1) was used without any correction. For post-dry pull-off (**Fig. S5**), the measured value of d*C*/dA is 0.42 times of the theoretical value calculated according to Eq. (2). Hence, predicted force is greater by a factor of 1.54.

Measurement of macroscale shear adhesion with a double-lap test setup using an Instron. This double-lap setup (**Fig. 3a**) was designed to resolve the issue of supporting substrate failure (*e.g.*, the necking of a PET film, as seen in **Fig. S7a**) prior to that of the adhesive itself, as well as to minimize unwanted failure modes of opening and out-of-plane shear. A Kevlar tendon can sustain a much higher force capacity as shown in **Fig. S8**. Specifically, our double-lap shear adhesive sample was designed to reliably capture high peak forces above 140 N (even for our smallest sample with area of ~ 0.25 cm^2). As seen in **Movie S1**, two 2 cm^2 samples (safety factor ~ 2 to minimize risks due to potential failures), which were attached to either side of a metal plate and in a double-lap configuration with the Kevlar tendons, *i.e.*, with an active PHEMA area of 4 cm^2, successfully supported the weight of an adult human, ~ 87 kg. The double-lap configuration with Kevlar "tendons" generated force (F) – displacement (d) curves with two peaks, indicative of two distinct adhesion-failure events (**Fig. S9**). In an ideal scenario, when the lengths of the two Kevlar tendons are equal ($l_A = l_B$), the load is shared equally upon tensile loading in an INSTRON®, resulting in a higher value of the first peak, $F_1^{lA=lB}$ (that corresponds to the failure of the first of the two lap joints), when compared to that of the second peak, $F_2^{lA=lB}$(*e.g.*, 346 N from a 0.5 cm^2 sample), as shown in **Fig. S9b**. However, an unavoidable mismatch in the lengths of Kevlar

tendons ($l_A \approx l_B$; $l_A \neq l_B$) forces the shorter of the two to first take up a disproportionate amount of the load, $F_1^{lA \neq lB}$. Regardless of the tendon length mismatch, following the first failure event, the test setup is less prone to opening mode failure and effectively reduces to a 'single-lap', 'single-tendon' test. Hence, the second peaks (both $F_2^{lA \approx lB}$ and $F_2^{lA \neq lB}$) provide a reasonable estimate of the strength of a single interface and is defined as the adhesion force measured in every test.

Characterization of the mechanical properties of other hydrogel systems and testing their macroscopic adhesive behaviors. To investigate whether PHEMA hydrogel is unique in its material class in its ability to satisfy all three critical criteria for reversible, superstrong shear adhesion, including self-tackiness and conformability in the wet state, small stored elastic energy upon drying, and a high dry state modulus, we prepared three sets of hydrogel samples, including two from PHEMA family, poly(2-hydroxyethyl methacrylate-*co*-methyl methacrylate) (PHEMA-*co*-PMMA) and poly(2-hydroxyethyl methacrylate-*co*-acrylic acid) (PHEMA-*co*-PAA) with varying copolymer ratios, and the conventional hydrogel, poly(ethylene glycol) diacrylate (PEGDA).

While most samples possessed near-surface wet state elastic moduli in the relative vicinity of (yet above) the Dahlquist criterion for tack (see **Fig. S12a-c**), which would permit conformability upon initial contact with a target surface, those with stiffer surfaces (see **Fig. S12d** from PHEMA-*co*-PAA, 10 vol % PAA) would severely hinder the conformal contact. All samples tested met the dry state high modulus requirement as seen in **Fig. S13**.

While diminished conformability provides a straightforward reason for the lack of macroscopic adhesion exhibited by stiffer hydrated variants, the negligible adhesion or complete lack thereof observed in all of our macroscopic tests irrespective of a desirable wet state modulus,

warrants a closer look at the phenomenon of residual stress minimization in the PHEMA system - which we infer as arising from the decoupling of Young's modulus, E, upon drying, from shrinkage. It is our understanding that unlike in PHEMA, the release of stored elastic strain energy (U) in most other soft hydrogels upon drying would preclude any observable adhesive behavior, which is also what makes PHEMA unique.

Imagine a film of hydrogel that is constrained by a stiff substrate. Let us say it undergoes shrinkage $\varepsilon(t)$ as a function of time but this shrinkage is disallowed due to the constraint of the substrate. Let us suppose that the tangent modulus grows as a function of strain as $E(\varepsilon) = E^f \left(\frac{\varepsilon}{\varepsilon^f}\right)^n$ where E^f is the final value of modulus, and ε^f is the final value of residual strain. If n=0, we have a constant value of modulus. If n>1, the modulus grows slowly in the beginning and quickly later. Conversely, if $n<1$ the modulus grows rapidly in the beginning and slowly in the later stage of drying. By definition, $E(\varepsilon) = \frac{d\sigma}{d\varepsilon}$, so $\sigma(\varepsilon) = E^f \left(\frac{1}{\varepsilon^f}\right)^n \frac{\varepsilon^{n+1}}{n+1}$ (since stress is zero at zero strain). Also, energy density $u = U/V$ is given by

$$u(\varepsilon) = \int \sigma(\varepsilon)\, d\varepsilon = \int E^f \left(\frac{1}{\varepsilon^f}\right)^n \frac{\varepsilon^{n+1}}{n+1}\, d\varepsilon = E^f \left(\frac{1}{\varepsilon^f}\right)^n \frac{\varepsilon^{n+2}}{(n+1)(n+2)} \qquad \text{(S7)}$$

Where V is the volume. If E is constant, $n=0$, and we retrieve the well-known expression for residual strain energy density, $\frac{E^f \varepsilon^2}{2}$. Of course, one can minimize residual energy density by minimizing residual strain. However, for a given residual strain and final modulus, consider the desirable case where modulus is not constant but builds up with shrinkage. In particular, note that as n increases, the residual energy density decreases. The ratio of residual energy density to that of the case of constant modulus (when the final modulus in the two cases is the same) is $\frac{2}{(n+1)(n+2)}$.

For large n, which corresponds physically to the situation where all the shrinkage occurs *before* the modulus increases, the residual energy density becomes vanishingly small.

This example shows that for residual energy density to be minimized, given some overall shrinkage and final value of dry modulus, it is desirable that shrinkage occur while E is a small number and that increase in E should occur after shrinkage is nearly complete. More commonly, however, this condition is not met in a typical hydrogel drying process, leading to large residual stress and energy. This phenomenon becomes evident when observing the drying process of a cross-patterned 180 μm thick PEGDA film (see **Movie S4**), which underwent catastrophic failure via fracture and delamination due to the release of relatively large amounts of stored elastic energy.

While the precise role of individual sample chemistry in mediating observed mechanical properties (and thereby adhesive behaviors) as well as the complexities of failure mechanisms in individual material systems will have to be confirmed in future studies, all our experimental evidence so far indirectly speaks to the importance of strain energy storage and wet state modulus as being the determining factors for whether a given hydrogel can behave as an adhesive or not.

Table S1. Adhesive Reversibility measured via repetitive indentation at the same spot on the flat PHEMA gel

Iteration	Maximum Pull-off Force measured (mN)	Wetting duration	Drying duration
1	163.37	Overnight	1 h
2	245.76	Overnight	1 h
3	257.62	1 h 40 min	1 h15 min
4	225.50	Over a weekend	1 h30 min
5	165.31	1 h	1 h8 min
6	186.80	Overnight	1 h18 min
7	133.27	1 h 30 min	1 h
8	205.66	Overnight	1 h15 min
9	176.06	1 h 50 min	1 h18 min
10	217.46	Overnight	1 h25 min
11	129.62	2 h	1 h27 min
12	203.94	Overnight	1 h16 min

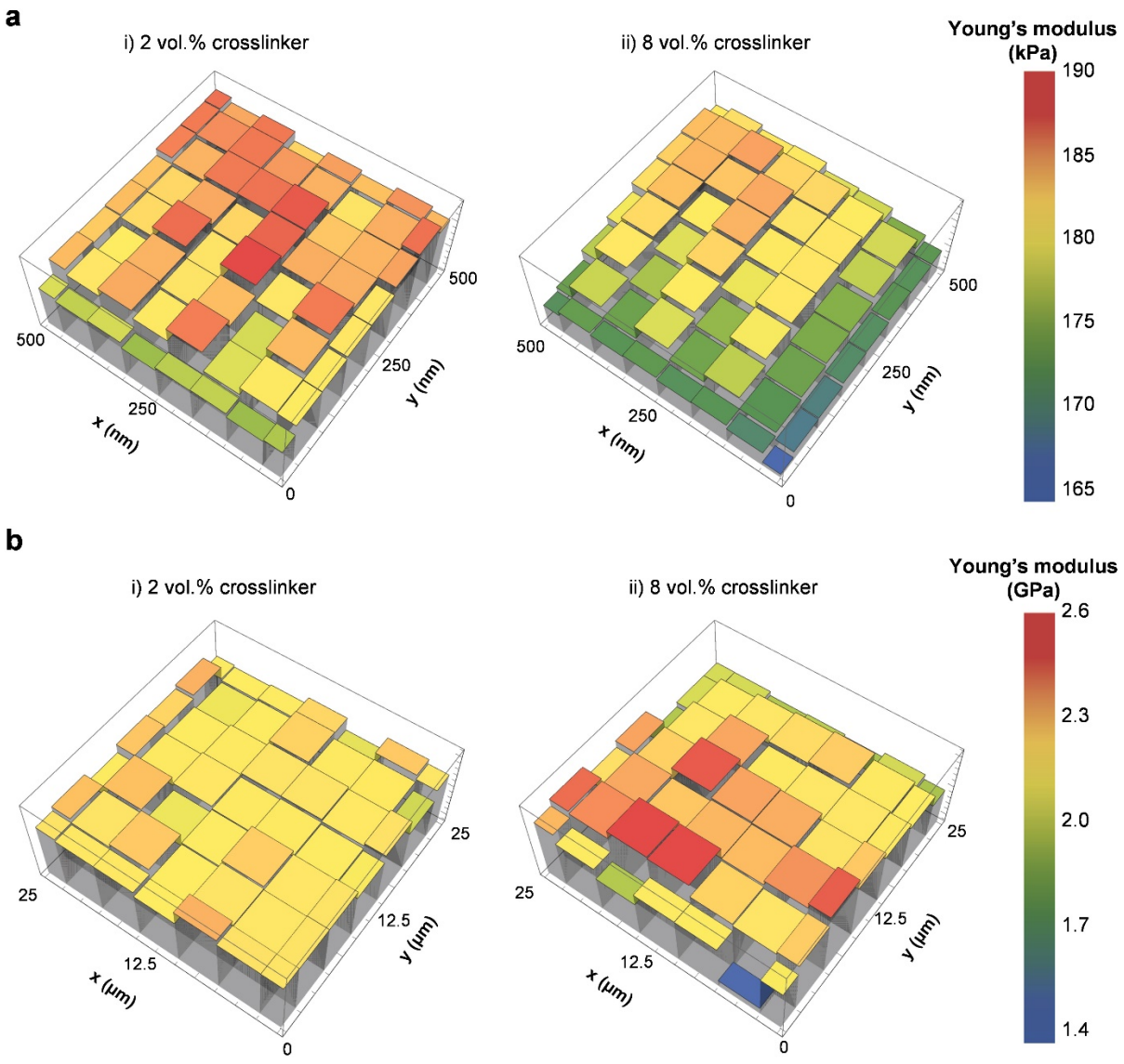

Fig. S1. Young's modulus of PHEMA hydrogel measured by AFM. (a-b), Near-surface elastic moduli of hydrogels in (a) wet state and (b) dry state with 2 vol % (left) and 8 vol % (right) of crosslinker, EDGMA, respectively.

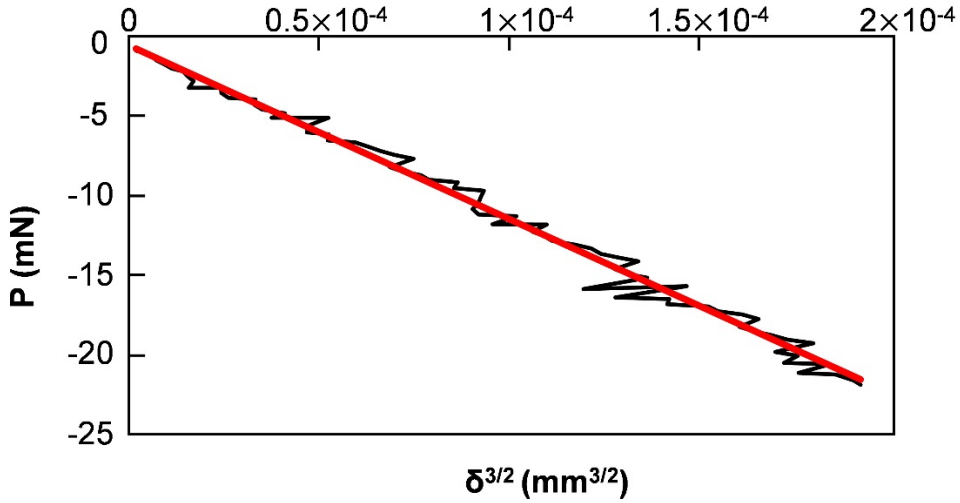

Fig. S2. Indentation on a flat, swollen PHEMA sample crosslinked with 8 vol% EDGMA under wet conditions. The resulting normal load (P) varies linearly with deflection to the 3/2 power ($\delta^{3/2}$), suggesting that over this range the contact is Hertzian. By fitting these data to the Hertz result, $E = \frac{9}{16\sqrt{R}}\frac{P}{\delta^{3/2}}$, provides an estimate of 34.9 MPa for the Young's modulus.

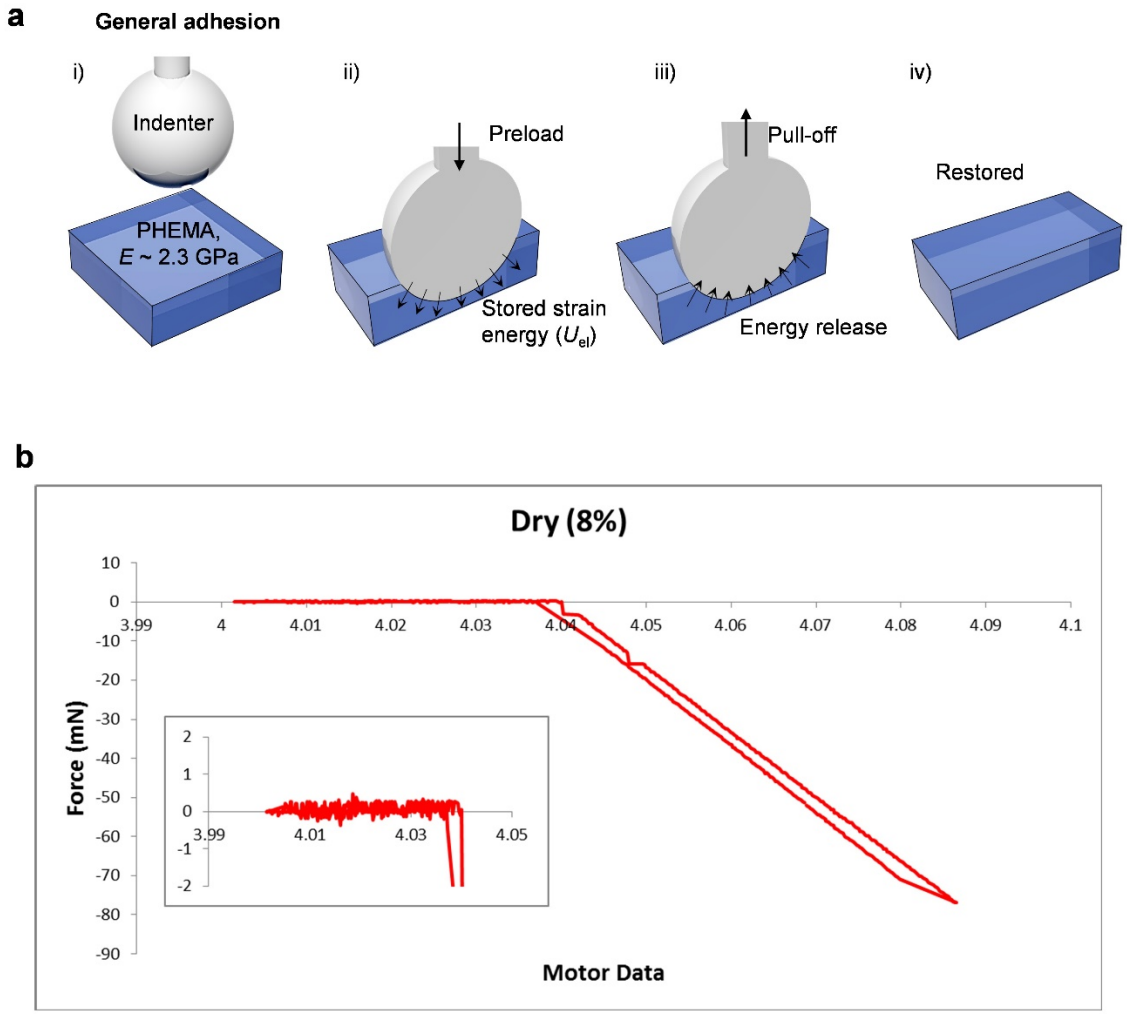

Fig. S3. Indentation on a dried PHEMA gel (with 8 vol% EDGMA) surface as a control. (a) An exaggerated illustration of a simple adhesion test via indentation performed on a dry, rigid PHEMA sample that does not exhibit any shape-memory. (b) Indentation experiments show no significant adhesion strength measured upon pull-off dry PHEMA gel.

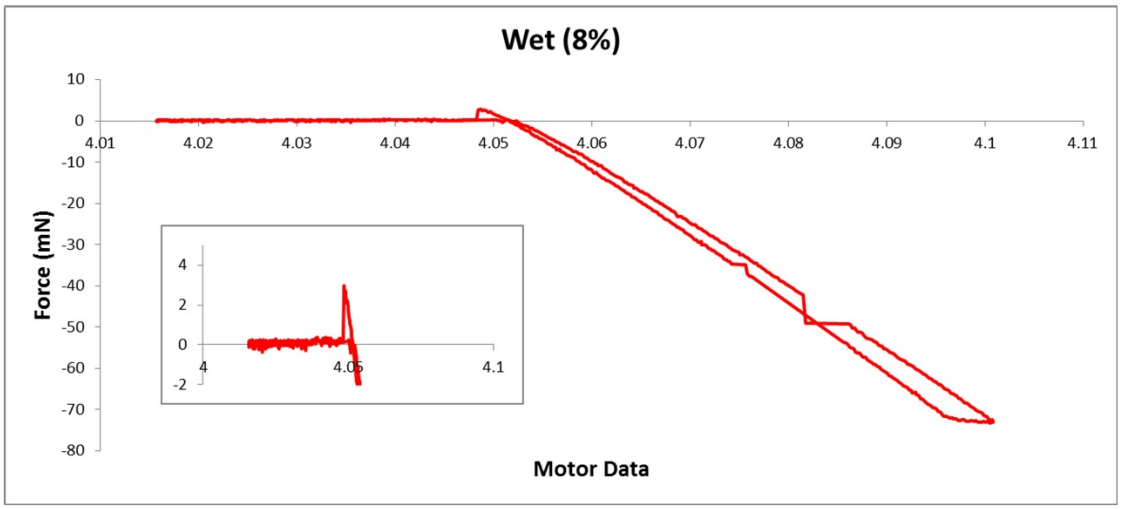

Fig. S4. Indentation on wet PHEMA surface (with 8 vol% EDGMA) as another control. The measured pull-off forces are slightly larger than those measured from the dry control sample but still about two orders of magnitude smaller than those measured after shape adaption upon *in situ* drying is allowed to occur.

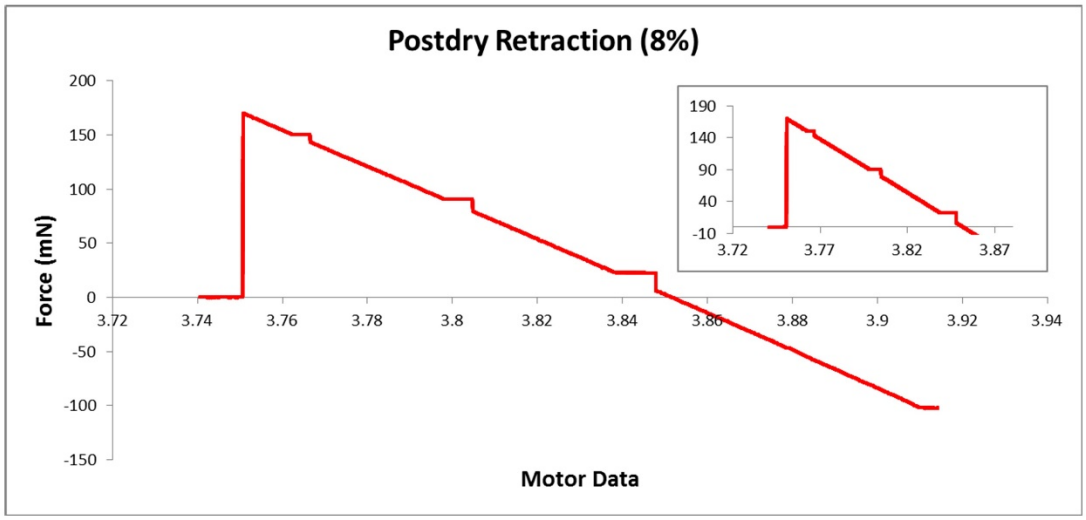

Fig. S5. Indentation performed by drying a wet PHEMA sample (with 8 vol% EDGMA) held in contact with an indenter under an applied preload. Significantly, the measured pull-off forces in this case are about two orders of magnitude higher than those measured on the controls as described earlier.

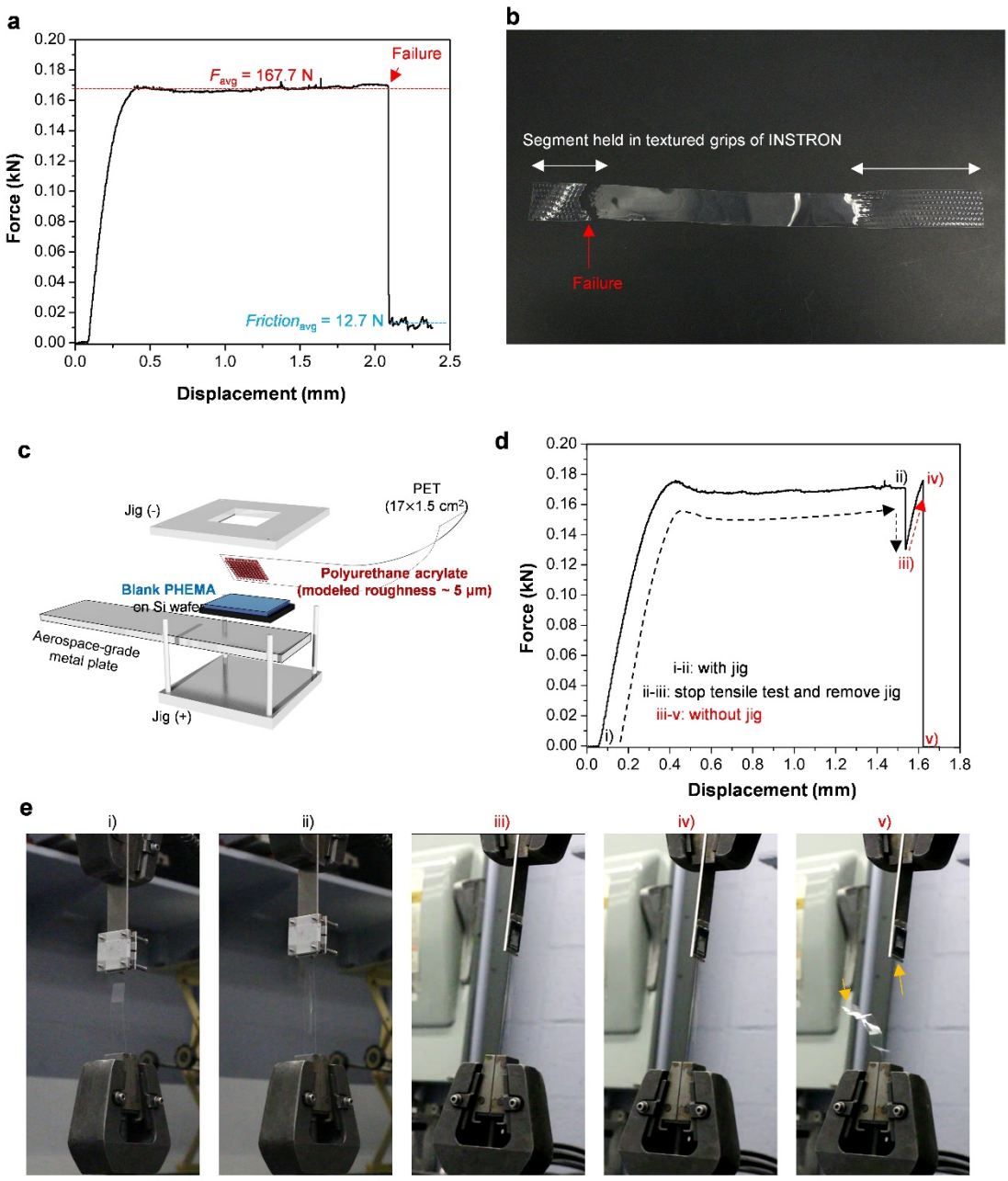

Fig. S6. Failure of PET film. (a-b) A PET film tested in tension using an INSTRON®, showing plastic deformation and fracture. Load-displacement curves, suggesting that a PET film would be ill-suited as a backbone of any adhesive system subjected to and capable of withstanding maximum loads exceeding ~ 160 N. (c-d) Failure of a PET film with a rough polyurethane acrylate (PUA) surface adhering, via an adhesive PHEMA superglue film, to a Si wafer that is in turn affixed to a

metal plate (c). Results of the tensile test (load-displacement curves) (d). (e) Initially, the compression jig used to maintain conformal contact of the mating surface with the adhesive during the drying process was not removed for the first part of the tensile test (from i to ii). This was done to avoid prestressing the sample prior to testing and also served to minimize loading in opening and out-of-plane shear modes *i.e.*, to test the sample in pure shear. After a point, the tensile test was paused, and the jig was disassembled while the sample was kept in tension. When the test was resumed, the applied tensile load (from iii to iv), caused the failure of the PET film (v). Note that adhesion and the adhesive interface was unaffected and survived the failure of the PET backbone.

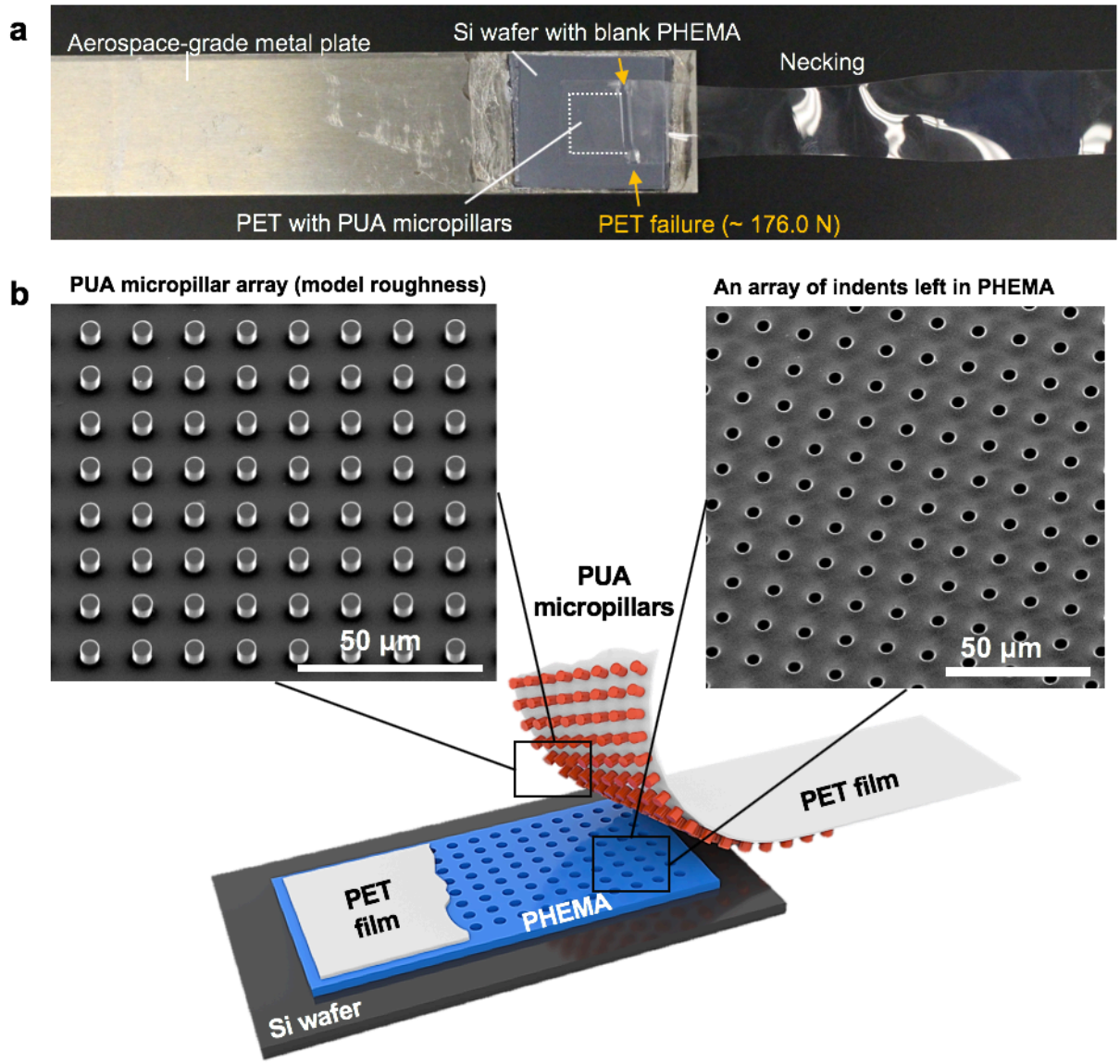

Fig. S7. Observation of shape adaption behavior in a PHEMA adhesive pad when forced to detach from a model rough target consisting of a square array of PUA micropillars. (a) PET backbone with PUA micropillars as described in Fig. S6, showed evidence of necking. When pulled in tension, sample failure was observed in the PET film and at the edge of the area in contact with the adhesive. (b) Illustration of the sample shown in (a). Evidence of shape adaption and shape memory behaviors in a PHEMA adhesive pad when forced to detach from a model rough target, a PUA micropillar array (5 μm in diameter and height and 10 μm in spacing) attached to a PET

substrate. Insets: SEM images of the PUA micropillars (left) and the dents left in the PHEMA adhesive (right).

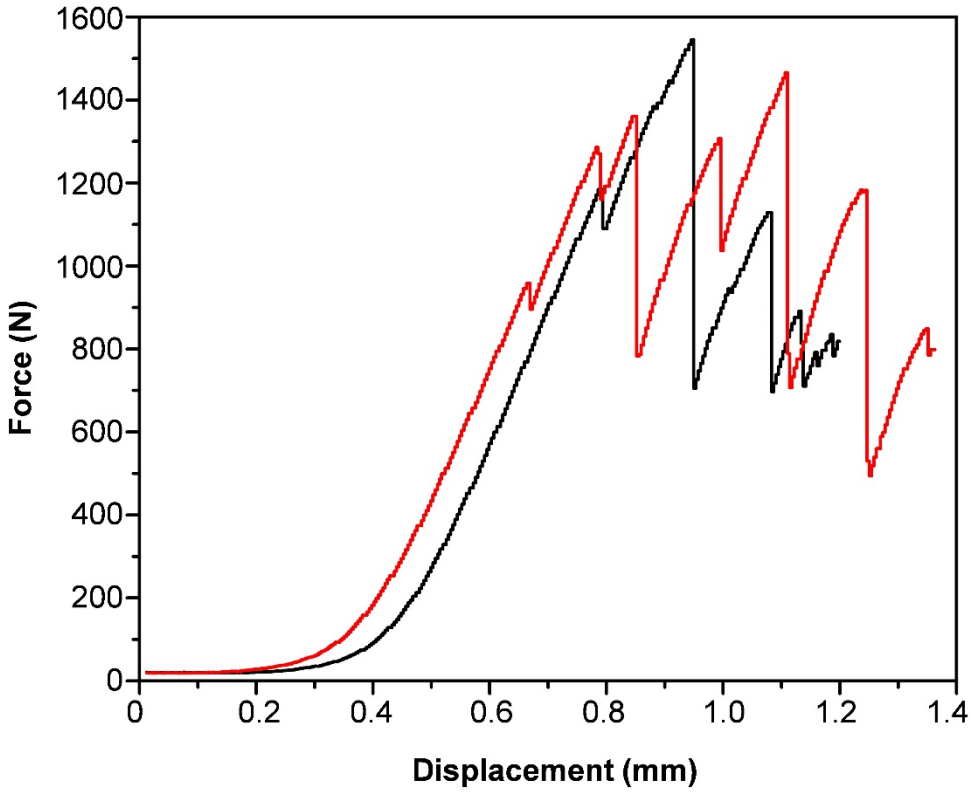

Fig. S8. Tensile tests of a single Kevlar® strap as a control, performed using an INSTRON®. The similar load-displacement curves from the two independent measurements made, suggest that the usage of Kevlar® as a low compliance (in-plane, tensile) tendon in this study, is valid up to a maximum shear adhesion force of ~ 1100 N. Beyond this point, multiple local failure events are observed in the woven Kevlar® tendon. Hence, the double-lap test setup employed in this work utilizes Kevlar tendons – which are sufficiently compliant when subjected to twisting or bending so as to minimize the effect of test setup misalignments and out-of-plane torsional stresses, while at the same time exhibiting low compliance when pulled in tension and not detracting from the system's low overall compliance. This allows us to reliably probe the force capacity of our hydrogel superglues.

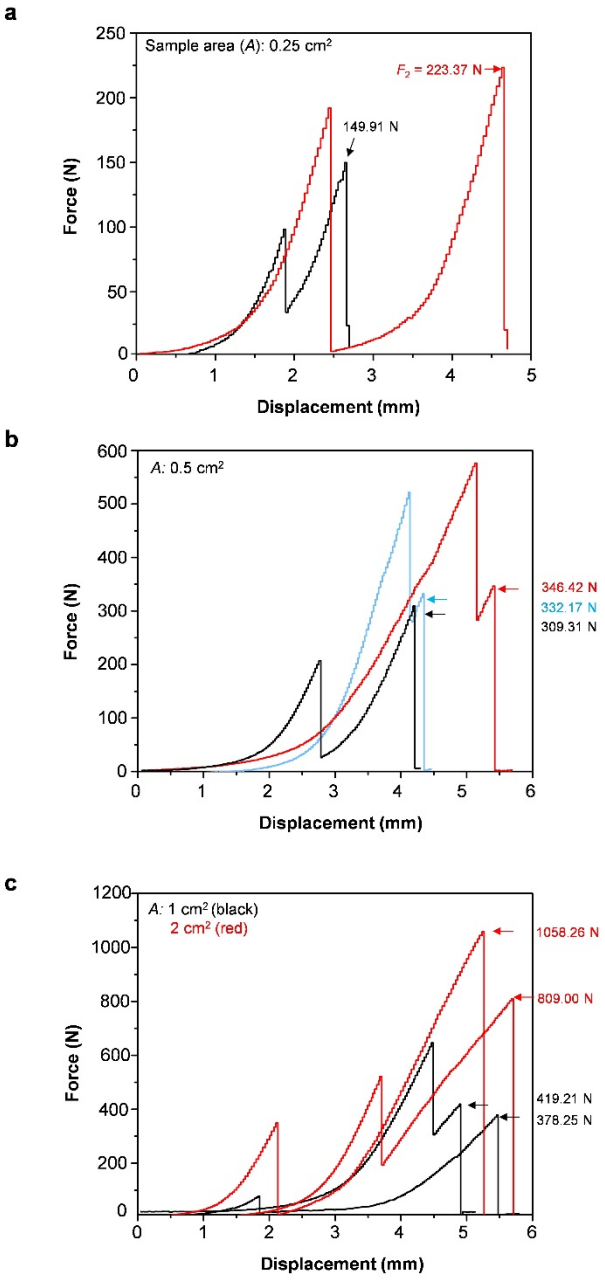

Fig. S9. Examples of force-displacement curves from the shear adhesion measurements performed on the double-lap test setup using an INSTRON® universal testing machine. The tested sample areas were 0.25, 0.5, 1, and 2 cm^2, respectively. See explanation in Supplementary Note 4.

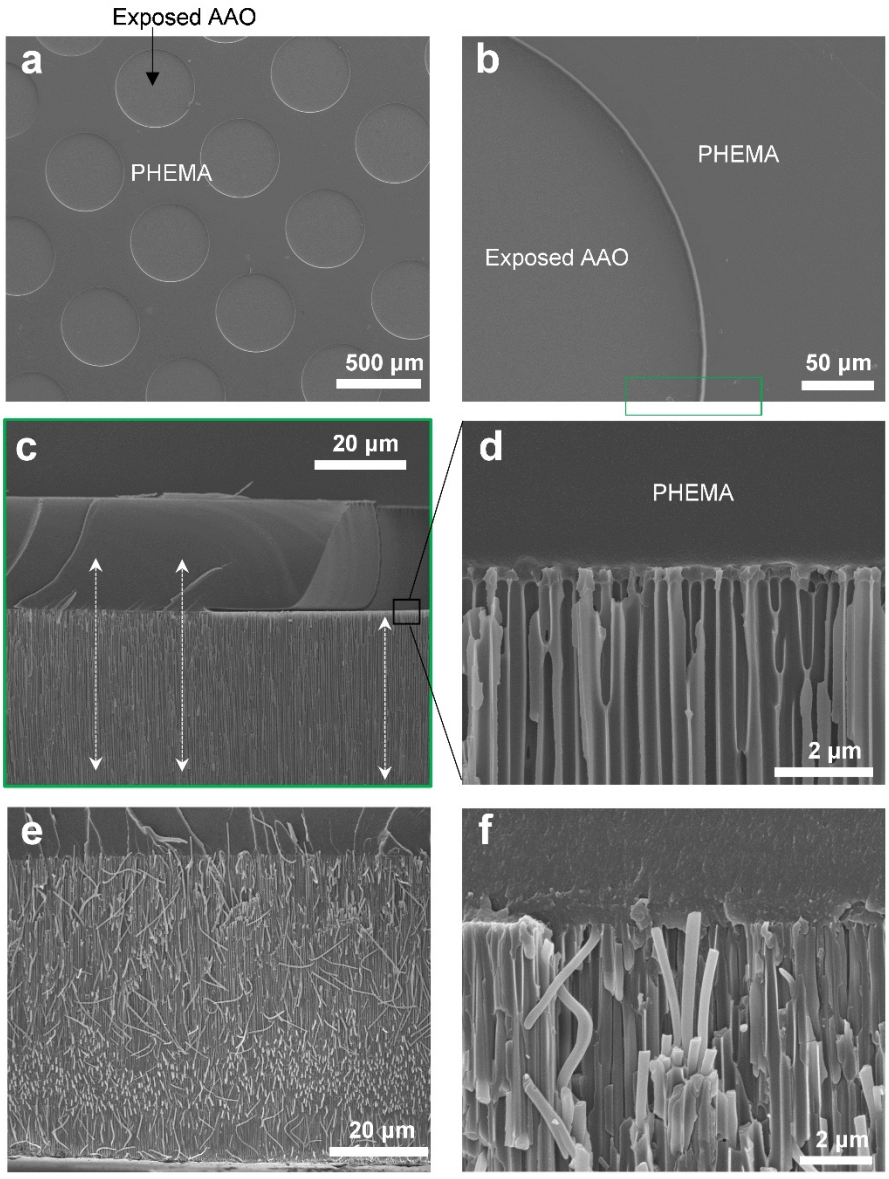

Fig. S10. SEM images of mesh-type hydrogel adhesives gluing two AAO membranes together. (a) A free-standing PHEMA membrane adhesive (500 μm in diameter and thickness through holes), is used to glue two AAO membranes. (b) A close-up SEM image of (a). (c) Cross-sectional view SEM image of the contact interface, clearly showing intact AAO nanochannels. The large microscale holes in the adhesive layer will ensure fluid transport through the AAO membrane without significant blockage. (d) The maximum depth to which the PHEMA gel is able to penetrate into AAO membrane is less than 100 nm, allowing for preservation of the nanochannels in the

AAO membrane. (e-f) Contamination of the AAO nanochannels by commercial superglues. (f) Magnification of (e).

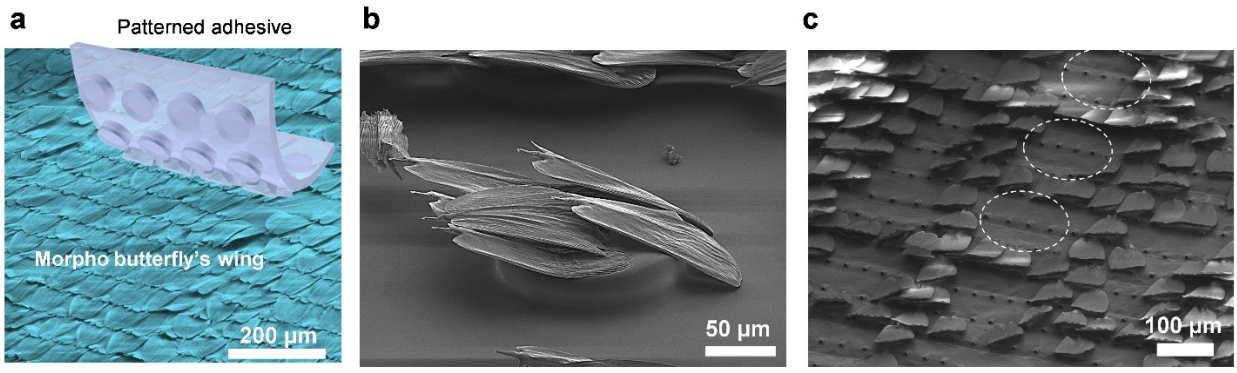

Fig. S11. Selective adhesion and detachment of butterfly wing scales using a patterned hydrogel pad. (a) Optical microscope image of Morpho Didius butterfly wing scales with an overlaid schematic of a hydrogel adhesive pad with a square array of dot patterns (diameter, 150 µm, spacing 300 µm, and height, 50 µm). Controlling the geometry of the contacting adhesive area allows for the selective detachment of scales from a morpho butterfly's wing. (b) SEM image showing the selectively detached scales adhere only to the dot patterns. (c) Optical microscope image of the morpho butterfly wing post-removal of the scales. The white dashed circles indicating the area of the wing previously in contact with the adhesive dots before their removal.

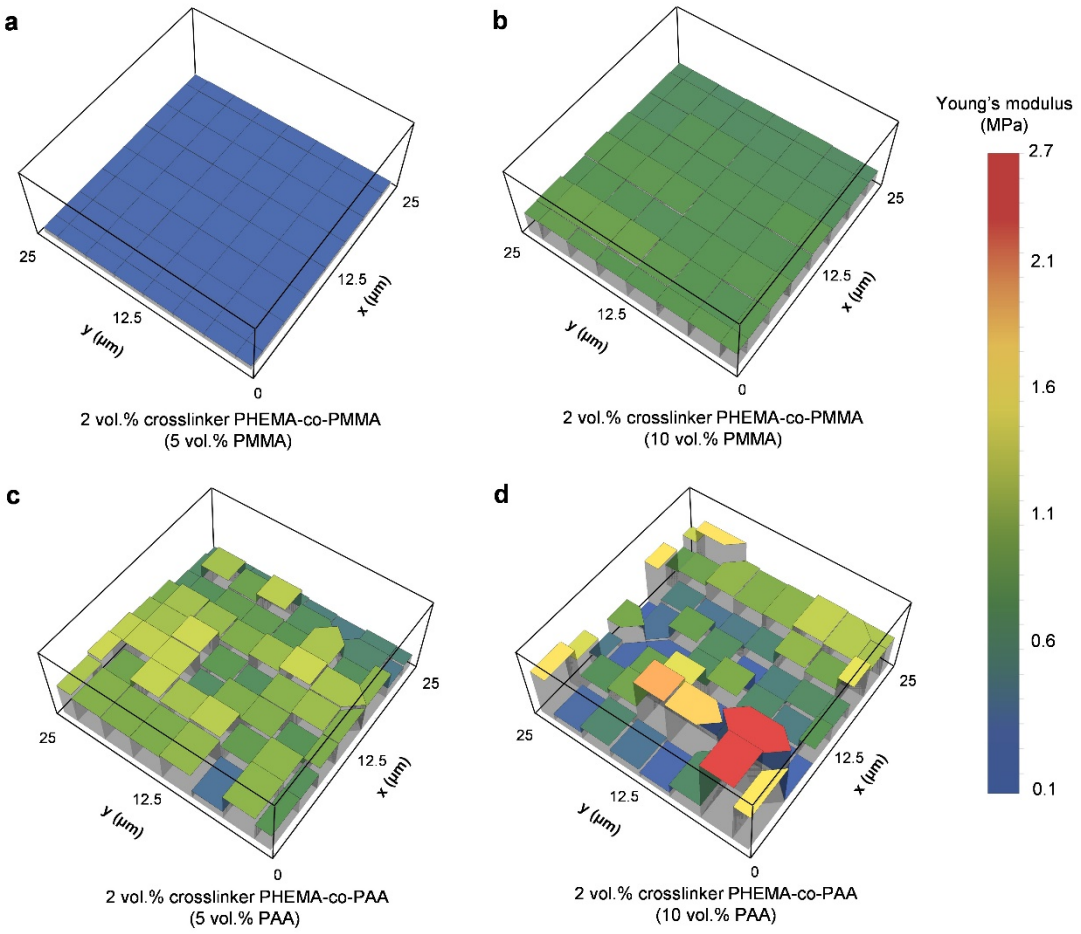

Fig. S12. Near-surface wet state Young's moduli of PHEMA-*co*-PMMA (a, b) and PHEMA-*co*-PAA (c, d) hydrogel films measured by AFM. (a) 5 vol % and (b) 10 vol % of PMMA. (c) 5 vol % and (d) 10 vol % of PAA. All cured with 2 vol % of crosslinker, EDGMA.

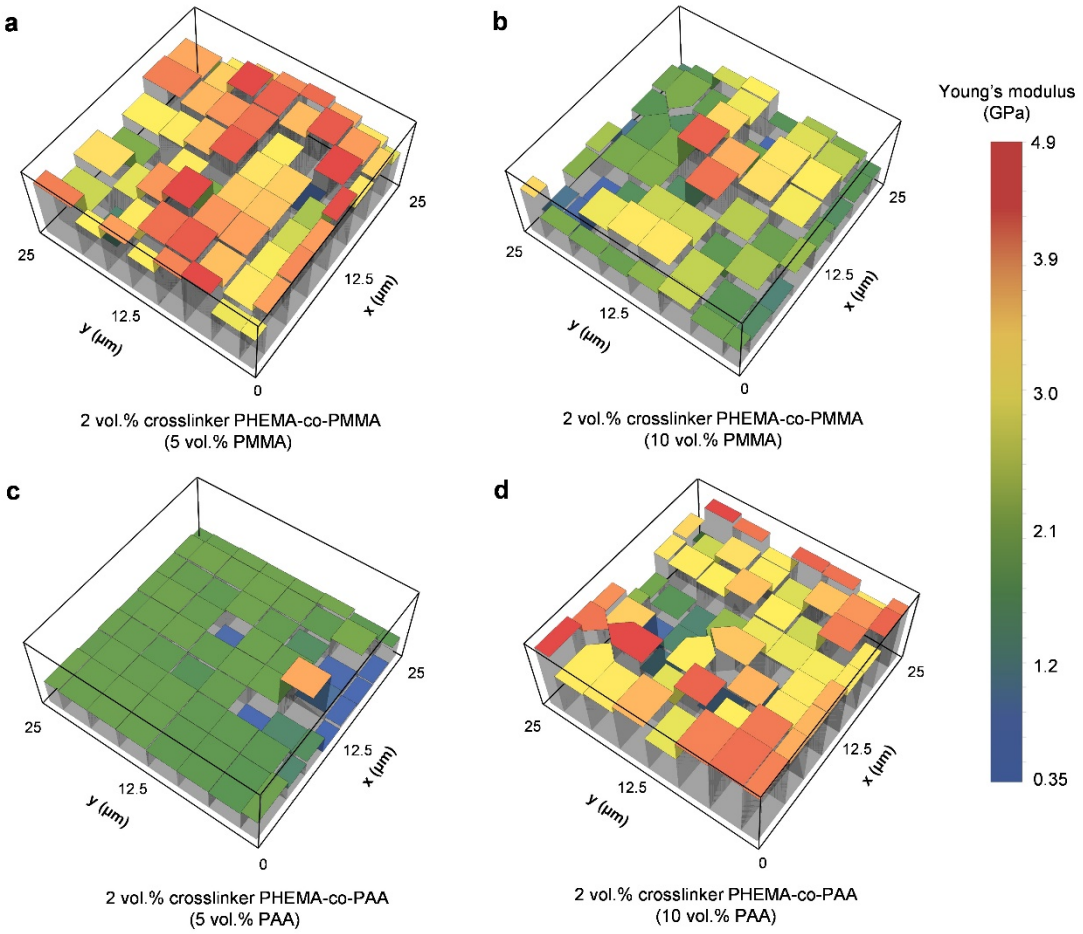

Fig. S13. Near-surface dry state Young's moduli of PHEMA-*co*-PMMA (a, b) and PHEMA-*co*-PAA (c, d) hydrogel films measured by AFM. (a) 5 vol % and (b) 10 vol % of PMMA. (c) 5 vol % and (d) 10 vol % of PAA. All cured with 2 vol % of crosslinker, EDGMA.

Movie S1. Human-scale load bearing test showing an adult human male weighing ~ 87 kg supported by two 2 cm^2 adhesive films in a double-lap configuration.

Movie S2. Self-detachment of two bonded glass substrates by rehydrating the hydrogel pad with a crossed pattern. Water was introduced at (0:10) and complete detachment was observed after 170 s.

Movie S3. Demonstration of rehydration-induced detachment of a flat PHEMA film cast on a Si wafer, which was bonded to a model rough target surface (PUA pattern on a single Kevlar® strip). A 4kg metal block was suspended from the tendon and water was introduced at the adhesive interface using a syringe at (0:37). Sample detachment was observed at (2:32).

Movie S4. Hydration-induced delamination and fracture of a 180 μm thick PEGDA hydrogel film molded with a cross pattern on a glass slide substrate as a demonstration of potentially unfavorable hydrogel behavior when used as an adhesive.

References

1. Adams G & Nosonovsky M (2000) Contact modeling—forces. *Tribology international* 33(5-6):431-442.
2. Johnson K, Kendall K, & Roberts A (1971) Surface energy and the contact of elastic solids. *Proc. R. Soc. Lond. A* 324(1558):301-313.
3. Lawn B & Wilshaw TR (1993) *Fracture of brittle solids* (Cambridge university press).
4. Vajpayee S, Hui C-Y, & Jagota A (2008) Model-independent extraction of adhesion energy from indentation experiments. *Langmuir* 24(17):9401-9409.
5. Long R, Hui C-Y, Kim S, & Sitti M (2008) Modeling the soft backing layer thickness effect on adhesion of elastic microfiber arrays. *J. Appl. Phys.* 104(4):044301.